J. Micromech. Microeng. **10** (2000) 459–465. Printed in the UK PII: S0960-1317(00)11502-5

Optimization of a circular piezoelectric bimorph for a micropump driver

Christopher J Morris and Fred K Forster†

Mechanical Engineering Department, Box 352600, University of Washington, Seattle, WA 98115, USA

E-mail: forster@u.washington.edu

Received 1 February 2000

Abstract. Piezoelectric bimorph actuation has been successfully used in numerous types of microdevices, most notably micropumps. However, even for the simple case of circular geometry, analytical treatments are severely limited. This study utilized the finite-element method to optimize the deflection of a circular bimorph consisting of a single piezoelectric actuator, bonding material and elastic plate of finite dimensions. Optimum actuator dimensions were determined for given plate dimensions, actuator-to-plate stiffness ratio and bonding layer thickness. Dimensional analysis was used to present the results for fixed- and pinned-edge conditions in a generalized form for use as a design tool. For an optimally-thick actuator, the optimum actuator-to-plate radius ratio ranged from 0.81 to 1.0, and was independent of the Young's modulus ratio. For thin plates, a bonding layer minimally affected the optimum dimensions. The optimized actuator dimensions based on a model of an actual device were within 13% of the fixed-edge condition.

1. Introduction

Piezoelectric bimorphs are used as micropump drivers, sound generating or receiving devices and general purpose displacement actuators. The simplest bimorph is made by bonding a piezoelectric element to one side of a passive elastic plate. When an electric field is applied across the thickness, the piezoelectric element strains transversely and radially. The radial strain causes the surface of the passive plate to expand or contract, which causes the entire bimorph structure to bend. The transverse displacement per volt obtained from a bimorph is typically much greater than that of bulk piezoelectric material. Bimorphs can also have two piezoelectric layers, or multiple piezo/elastic layers. The single-piezoelectric-layer configuration, which is the configuration used in this study, has been referred to as a 'unimorph' (Lee and Marcus 1981, Smits *et al* 1991), although this term is not widely used.

Much work was carried out in order to predict and optimize the behavior of multiple-layered piezoelectric bimorphs in the Cartesian domain. The cantilever beam has been analyzed extensively in two dimensions (Lee and Marcus 1981, Smits *et al* 1991, Meng *et al* 1993). A three-dimensional analytical analysis for rectangular, simply-supported, multiple-layer, laminated piezoelectric/passive plates is given by Ray *et al* (1993). Shah *et al* (1993) also numerically investigated simply-supported plates using a finite-element formulation, including different shapes of piezoelectric patches. Batra *et al* (1996) conclude that when the purpose of piezoelectric patches is to damp out vibrations, the optimum placement of the patches are at the locations of the plate's maximum displacement under free vibration. Kim and Jones (1991) used thin plate theory to predict optimum actuator-to-plate thickness ratios at different Young's modulus ratios by optimizing the moment applied by a dual-layer piezoelectric actuator. Chaudhry and Rogers (1994) also present an argument for determining the optimum thickness ratio, explaining that including externally-applied moments greatly affects the result. They also predict optimum length ratios for a rectangular actuator patch on a rectangular plate with fixed edges, with the fixed-edge condition being equivalent to an externally-applied moment. The optimum actuator-to-plate length ratio is predicted as 0.62. Such analyses are vital to the understanding of bimorph behavior, but analyses based on Cartesian geometry cannot necessarily be applied to the circular case.

At least two works have analyzed bimorphs in the circular domain. Dobrucki and Pruchnicki (1997) develop a finite-element method for axisymmetric, circular plates. An analytical relation is also presented, which only holds for the displacement of a bimorph with the piezoelectric element covering the entire elastic plate. Also, the analysis assumes free edges and a dual-layer, symmetric actuator. Yanagisawa and Nakagawa (1993) present an analytical method for optimizing the radius of a resonating piezoelectric actuator for a limited number of thickness ratios and one

† Corresponding author.

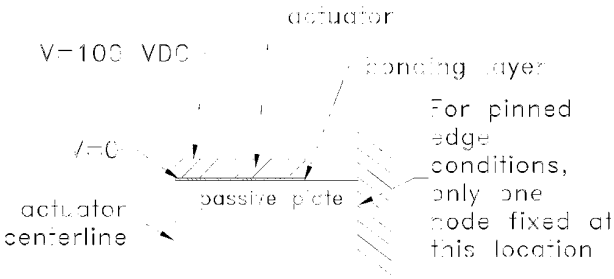

Figure 1. Geometry and idealized boundary conditions for a circular, single-actuator bimorph.

choice of material constants. For readers seeking further information on piezoelectric bimorphs, Chee *et al* (1998) present an extensive review on the analytical and numerical approaches to modeling actuator behavior.

It is surprising that the simple case of a single circular piezoelectric element bonded to a circular plate has not been analyzed in closed form for static actuation. Such a closed-form analysis would be complicated by the lack of symmetry about the neutral plane of bending. An analytical approach would be especially difficult if additional bonding layer and non-ideal edge conditions were included. Such an analysis therefore lends itself to the finite-element method, which can easily account for all of these factors, and can be used to optimize transverse or volumetric displacement.

2. Methods

2.1. Finite-element analysis model formulation

A static, two-dimensional axisymmetric finite-element model of a bimorph was developed based on the geometry shown in figure 1. The model included the actuator, bonding layer and passive plate. Idealized edge conditions were either (1) fixed, or (2) pinned by fixing one node at the centerline of the passive plate. A non-idealized edge condition model was also investigated, as discussed in section 2.2. The idealized model was used to calculate the effects of the plate radius-to-thickness ratio α, and the actuator-to-plate Young's modulus ratio β on the optimum actuator dimensions. The effects of bonding layer-to-plate thickness ratio ρ were also investigated.

The static analysis is justified when frequencies of operation are much less than the resonant frequency of the actuator-plate assembly. For example, when used as the driving element in a micropump designed for liquid transport, the typical operating frequency is in the low kilohertz range, while the free-air resonance is 10–30 times higher. The effect of pressure loading (micropump) or point loading (generic actuator) during actuation of the bimorph is assumed to not affect the determination of optimum actuator dimensions. This is an accurate assumption as long as the magnitudes of the load and actuation voltage are small enough so that their combined effect on the transverse displacements is linear. This condition exists if the displacement is small enough to be unaffected by in-plane stresses.

The finite-element analysis (FEA) program ANSYS 5.5 (Canonsburg, PA) was used to implement the model. Approximately 1300 axisymmetric PLANE13 elements were used, but the number varied with geometry. These four-node, two-dimensional bricks allowed degrees of freedom for radial and transverse displacement, and voltage potential. The underlying equations solved were the coupled linear piezoelectric equations, in terms of the piezoelectric matrix **e**. This form of the equations relates the electric field vector to the stress vector (Meng *et al* 1993). The matrix equation used by the finite-element solver was then

$$\begin{bmatrix} \mathbf{K} & \mathbf{K}^Z \\ (\mathbf{K}^Z)^T & \mathbf{K}^d \end{bmatrix} \begin{bmatrix} \boldsymbol{u} \\ \boldsymbol{V} \end{bmatrix} = \begin{bmatrix} \boldsymbol{F} \\ \boldsymbol{L} \end{bmatrix} \tag{1}$$

where the $\mathbf{K}$, $\mathbf{K}^d$ and $\mathbf{K}^Z$ matrices were formed by volume integrals of the structural stiffness, the dielectric conductivity and the piezoelectric coupling matrix, respectively. In each of these integrals, shape functions are used to approximate the distribution of the displacement and electric potentials across an element. The $\boldsymbol{u}$ and $\boldsymbol{V}$ vectors in equation (1) represent nodal displacements and voltages, while $\boldsymbol{F}$ and $\boldsymbol{L}$ are vectors of applied nodal forces and charges (*ANSYS Theory Reference* 1998).

The piezoelectric properties for PZT-5A (PSI-5A-S2, Piezo Systems, Cambridge, MA) were obtained from Jaffe and Berlincourt (1965) and Auld (1973). The latter source contains information on PZT-5H and was used because one of the six unique elasticity constants for PZT-5A ($s_{13} = s_{23}$) is not specified in Jaffe and Berlincourt. This seemed reasonable because the other *elastic* coefficients for PZT-5A and PZT-5H are within 20%. The complete, three-dimensional piezoelectric properties for PZT-5A are presented in table 1 for an element poled along the z-axis. For this study, the two-dimensional subset of table 1 was used, with the x and y directions being equivalent to radial and transverse directions, respectively.

The non-piezoelectric materials in the model were chosen to correspond to materials used for prototype devices. Conductive epoxy (EPO-TEK H31, Epoxy Technology, Billerica, MA) was used for the actuator bonding layer, with a Young's Modulus $E_b = 5.17 \times 10^9$ Pa, and a Poisson's ratio $\nu_b = 0.3$. For the passive plate, $\nu_p = 0.2$ was used, which corresponds to Pyrex (Borofloat, US Precision Glass, Elgin, IL). The passive-plate Young's modulus E_p was adjusted for the desired value of β, where $\beta = 0.968$ corresponds to Pyrex.

2.2. Model verification by analytical and experimental methods

To determine the accuracy of the finite-element approach, a two-dimensional plane-strain FEA model of a bimorph cantilever beam having a single piezoelectric layer was generated, having similar materials, geometry and mesh density to the idealized-edge circular model in figure 1. The calculated displacement was compared to the analytical prediction presented by Meng *et al* (1993, equation (42)), which was developed using composite-layer mechanics theory.

The FEA model of the circular bimorph was also compared to measured displacements of a circular micropump actuator. While driving the actuator with a sine wave, velocity measurements were integrated to obtain

Table 1. Piezoelectric material properties for the three-dimensional characterization of PZT-5A, with the poling direction along the z-axis.

Property	tensor (in order of x, y, z, xy, yz and xz)
Piezoelectricity $\mathbf{e}$ (C m^{-2})	$\begin{bmatrix} 0 & 0 & -5.4 \\ 0 & 0 & -5.4 \\ 0 & 0 & 15.8 \\ 0 & 0 & 0 \\ 0 & 12.3 & 0 \\ 12.3 & 0 & 0 \end{bmatrix}$
Permittivity ϵ (F m^{-1})	$10^{-9} \times \begin{bmatrix} 8.107 & 0 & 0 \\ 0 & 8.107 & 0 \\ 0 & 0 & 7.346 \end{bmatrix}$
Compliance $\boldsymbol{S}$ (m^2 N^{-1})	$10^{-12} \times \begin{bmatrix} 16.4 & -5.75 & -8.45 & 0 & 0 & 0 \\ & 16.4 & -8.45 & 0 & 0 & 0 \\ & & 18.8 & 0 & 0 & 0 \\ & \text{symmetric} & & 44.3 & 0 & 0 \\ & & & & 47.5 & 0 \\ & & & & & 47.5 \end{bmatrix}$

the displacement data. The velocity measurements were recorded using a laser vibrometer (OFV 302, PolyTec, Waldbronn, Germany). Three air-filled pumps each with 3 and 6 mm chamber diameters were tested at 3000 Hz and 200 V peak-to-peak to obtain the centerline displacement. The displacement across the entire chamber of two 6 mm diameter pumps was also taken at 100 V peak-to-peak, using an electronically controlled stage (855C, Newport Corporation, Irvine, CA) to position the pump for each displacement reading. These experimental data were then compared to FEA results for equivalent (zero-to-peak) static actuation. The resonant frequencies of these devices were in the 100 kHz range, so inertial effects were assumed negligible.

A 'non-idealized' FEA model was developed to include the effect of realistic, passive-plate edge support. A silicon edge support, corresponding to a micropump housing, was modeled with additional finite elements using $E = 1.3 \times 10^{11}$ Pa and $\nu = 0.22$. The non-idealized model then had approximately 1500 elements.

2.3. Optimization

A high-level routine in ANSYS called the first-order method was used to optimize the actuator-to-plate radius and thickness ratios, r^* and t^*. For each iteration, the gradient of an objective function was computed in the design space defined by r^* and t^*, the value of which determined the search direction to minimize the objective function. The objective function was defined as the reciprocal of either the actuator centerline or volumetric displacement. The optimum values $(r^*)_{opt}$ and $(t^*)_{opt}$ corresponded to the minimized objective function using a tolerance of 1.5×10^{-4} times the objective function.

Constraints were set on the applied voltage, using the maximum allowable electric field for PZT-5A across its poling axis, 5.24×10^5 V m^{-1} (Zhang *et al* 1995, figure 8(a)). For the non-idealized micropump model, constraints were also set on allowable stresses in the actuator, plate and bonding layer elements, as determined by the Von Mises stress theory.

2.4. Dimensional analysis

The optimization of piezoelectric actuator dimensions for both fixed- and pinned-edge conditions was carried out for several different values of α, β and ρ. Dimensional analysis was used to minimize the number of parameters needed to describe the results and to maximize their usefulness. For the case of optimum actuator radius the entire set of parameters considered can be expressed by the functional relation

$$(r_a)_{opt} = f(t_b, E_b, \nu_b, r_p, t_p, E_p, \nu_p, E_a, \nu_a, [\boldsymbol{e}, \boldsymbol{\epsilon}, \boldsymbol{S}]_a) \tag{2}$$

where the subscripts b, p and a represent the bonding layer, passive plate and actuator properties, respectively. Before dimensional analysis was applied, certain assumptions were made. First the analysis was limited to PZT-5A, so that the functional relationship of $(r_a)_{opt}$ to the piezoelectric properties could be ignored. The effect of Poisson's ratio was also ignored, because these values were not expected to vary over a wide range. Lastly, for the initial set of results, the bonding layer was ignored. With these considerations the expression for $(r_a)_{opt}$ is given by

$$(r_a)_{opt} = f(E_p, t_p, r_p, E_a). \tag{3}$$

Dimensional analysis was carried out on the above equation using the Buckingham method (Szücs 1980). Because equation (3) expresses a relationship between five parameters in combinations of only two units (length and pressure), it can be reduced to a functional relation between three non-dimensional Π parameters

$$\Pi_1 = g(\Pi_2, \Pi_3). \tag{4}$$

For the specific dimensional parameters in equation (3),

$$(\alpha)(r^*)_{opt} = g_1(\alpha, \beta). \tag{5}$$

The optimum actuator thickness $(t_a)_{opt}$ was also expected to be a function of the same parameters as in equation (2), in which case dimensional analysis yielded

$$(t^*)_{opt} = g_2(\alpha, \beta). \tag{6}$$

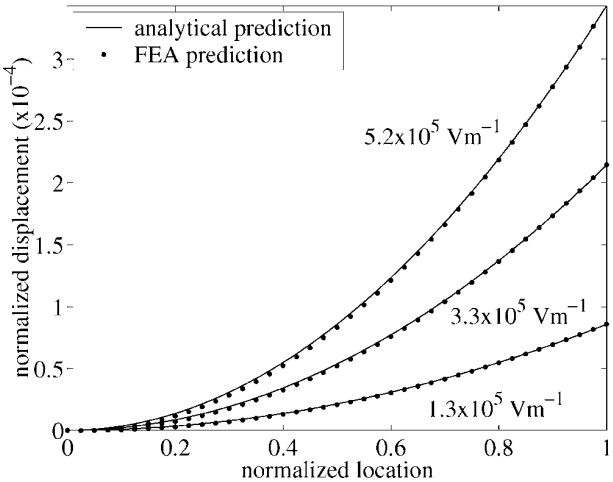

Figure 2. Displacement against location normalized by beam length of a single-piezoelectric-layer cantilever beam, as predicted by the analytical and finite-element methods, for various electric field strengths.

However, another non-dimensional relation was also considered based on the observation that the passive-plate stiffness coefficient $D_p = E_p t_p^3/[12(1-\nu_p^2)]$ contains E_p and t_p as the product, $E_p t_p^3$. Assuming the functional relation for $(t^*)_{opt}$ contained only that combination of E_p and t_p, the Buckingham method reduced the functional relation to two Π parameters:

$$\left(\frac{1}{\alpha}\right)(t^*)_{opt} = g_3\left(\frac{D_p}{E_a r_p^3}\right) = g_3(D^*). \tag{7}$$

The explicit form of equations (5) and (7) were determined from FEA.

Where appropriate, the results of actuator optimization in terms of the non-dimensional parameters given in equations (5) and (7) were fit with polynomials based on the least-squares error methods.

3. Results and discussion

3.1. Optimization of a circular bimorph with idealized edge support

The displacement of a cantilever beam was compared to an analytical prediction to verify the accuracy of the FEA program. Figure 2 shows this displacement, as a function of the beam length factor, as predicted by analytical and numerical methods. Excellent agreement was obtained for the various applied electric fields.

For a circular PZT-5A piezoelectric bimorph of different plate sizes and materials, the optimum actuator dimensions were computed. The results for optimum radius are shown in non-dimensional form in figure 3. Although equation (5) predicts a functional relationship depending upon α and β, the data in figure 3 could be considered as a function of α only, resulting in the following design equations:

$$(r^*)_{opt,fixed} = 0.814 + (0.410)\alpha^{-1}$$

$$(r^*)_{opt,pinned} = 1.0. \tag{8}$$

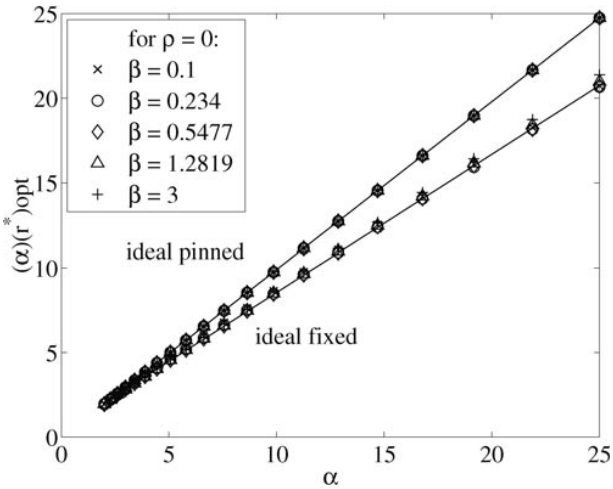

Figure 3. The product $(\alpha)(r^*)_{opt}$ for maximum centerline displacement against plate radius-to-thickness aspect ratio α, at various actuator-to-plate Young's modulus ratios β, as predicted by the FEA model. The lines shown are polynomial expressions given by equations (8).

For the fixed model, $(r^*)_{opt,fixed}$ decreased with increasing α, but it was always greater than 0.8. The departure from unity means thinner passive-plates require more bare region to achieve maximum displacement. The result for $(r^*)_{opt,pinned}$ being unity can be explained by considering the actuation to be equivalent to a line moment located at its radial boundary (an assumption made in many analyses), in which case a moment located at the plate edge will cause the most deflection (Roark 1989, p 364).

Unlike $(r^*)_{opt}$, the data for $(t^*)_{opt}$ exhibited a strong dependence on both α and β as generally expected according to equation (6). Alternatively equation (7) was used for the results shown in figure 4. The weak dependence upon β indicates that the assumptions used to obtain equation (6) are valid. The data was considered compact enough to fit the curves shown in the figure. The design equations based on these results are:

$$(t^*)_{opt,fixed} = \alpha[\exp(-0.001\,195\xi^3 - 0.037\,92\xi^2 - 0.046\,96\xi - 0.5365)]$$

$$(t^*)_{opt,pinned} = \alpha[\exp(-0.000\,3856\xi^3 - 0.005\,703\xi^2 + 0.3584\xi + 0.055\,97)] \tag{9}$$

where $\xi = \ln D^*$.

The results for maximum net volume displacement were also calculated, but not shown. The effect of optimizing the displaced volume was that $(r^*)_{opt}$ increased between 5 and 10% of the fixed-edge data shown in figure 3. The optimum thickness for a fixed-edge plate also increased between 5 and 15% over the range of parameters shown in figure 4. The optimum values for the pinned-edge case were unchanged.

It should be noted that the optimum dimensions from figures 3 and 4 should be used with care, because allowable stresses may be exceeded. The allowable stresses depend entirely upon the materials, and the investigation of every possible material is beyond the scope of this study. A non-dimensionalization scheme for the stresses similar to that for the optimum dimensions was applied, but the results

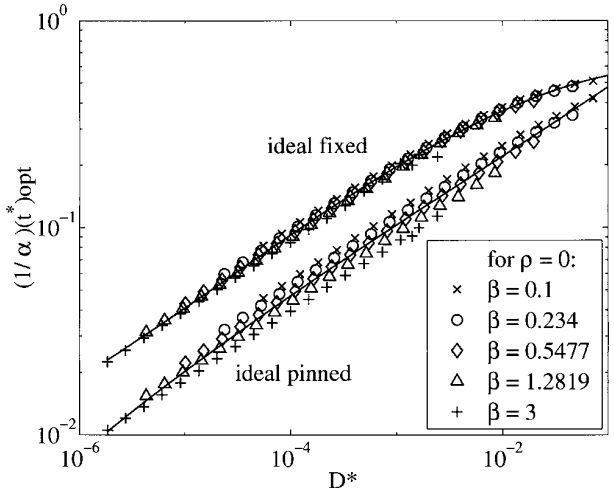

Figure 4. The product $(1/\alpha)(t^*)$ for maximum centerline displacement against non-dimensional plate stiffness D^*, as predicted by the FEA model at different actuator-to-plate Young's modulus ratios β. $D^* = D_p/(E_p r_p^3)$. Lines shown are polynomial expressions given by equations (9).

indicated that there were other factors affecting the maximum stresses. Therefore a summary figure showing the maximum stresses in an arbitrary bimorph is not presented. However, general guidelines are given. For the pinned-edge condition, the maximum stresses will generally not be exceeded. For the fixed-edge condition, $\alpha < 5$, and allowable passive-plate stresses less than 60 MPa, a sub-optimum-sized actuator may be required.

The results presented thus far have concerned bimorphs with no bonding layer, but most actual devices contain some bonding material, often a conductive epoxy. The effect of the bonding layer is one of the more interesting aspects to study with an FEA model. Figures 5 and 6 depict the optimum actuator radius and thickness ratios against the appropriate non-dimensional abscissa, at different values of ρ. Since figures 3 and 4 demonstrate that the effect of β is minimal, figures 5–7 were produced with one value of $\beta = 0.968$. The range of ρ considered is large; for most applications $\rho > 0.1$ would correspond to a substantially thick bonding layer. Nevertheless, the bonding layer has only a mild effect on $(r^*)_{opt}$ throughout the range shown in figure 5. For $D^* < 10^{-3}$ in figure 6, ρ also minimally affected $(t^*)_{opt}$. Noting that $D^* \propto (1/\alpha^3)$, ρ generally had a mild effect on the optimum dimensions for thin plates.

While the results shown in figures 5 and 6 give guidelines for optimizing a circular actuator with a finite value of ρ, it must be noted that displacement decreases with increasing bonding layer thickness. The magnitude of the effect is shown in figure 7. The reduction in displacement is most pronounced for thinner plates (small values of D^*).

For a general understanding of the behavior of the actuator, and to give an idea of how sensitive actuator displacement is to r^* and t^*, these parameters were varied on the idealized FEA model, with $\alpha = 6$, $D^* = 4.15 \times 10^{-4}$ and $\rho = 0$. Figure 8 shows the centerline displacement, normalized by the passive plate radius, of a pinned-edge actuator against r^* at several values of t^*. The displacement increased with increasing piezoelectric radius for all cases.

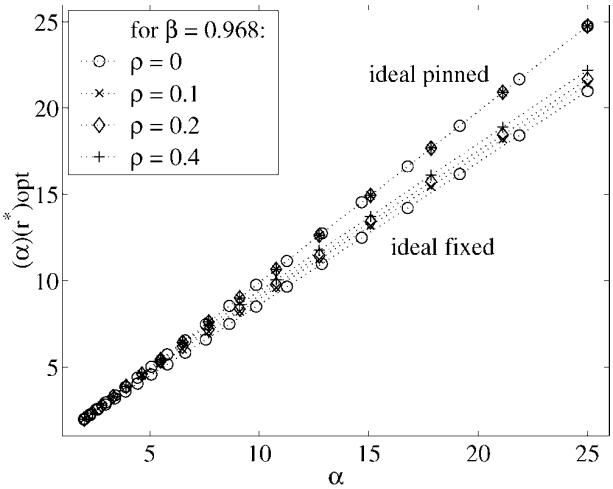

Figure 5. The product $(\alpha)(r^*)$ for optimum centerline displacement against plate radius-to-thickness ratio α, at different bonding-to-plate thickness ratios ρ. The lines between symbols are drawn for clarity.

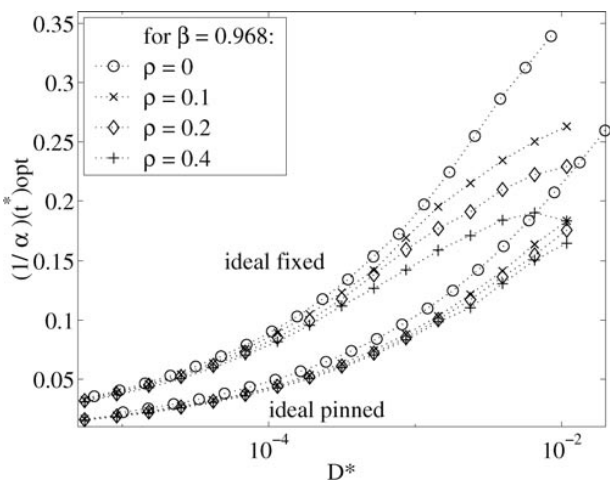

Figure 6. The product $(1/\alpha)(t^*)$ for maximum centerline displacement against non-dimensional plate stiffness D^*, at different bonding-to-plate thickness ratios ρ. The curves between the symbols are drawn for clarity.

Figure 9 shows the corresponding results for the fixed-edge condition. The optimum radius is apparent by the location of each curve's maximum, which increased with increasing thickness.

3.2. Effect of non-idealized edge support

As an example of an actual application, the piezoelectric actuator dimensions were optimized for two different sized micropump drivers. The passive plate thicknesses were predetermined from linear system analysis to yield a high fluid output at the system resonance frequency of 3000 Hz (Bardell *et al* 1997), so that $\alpha = 6$ and $D^* = 4.15 \times 10^{-4}$. The predicted deflection of a 6 mm diameter pump prior to optimization is compared with experimental data in figure 10. For this pump ρ was measured to be 0.04. Good agreement was obtained for the FEA model that utilized the non-ideal edge condition, although the idealized fixed-

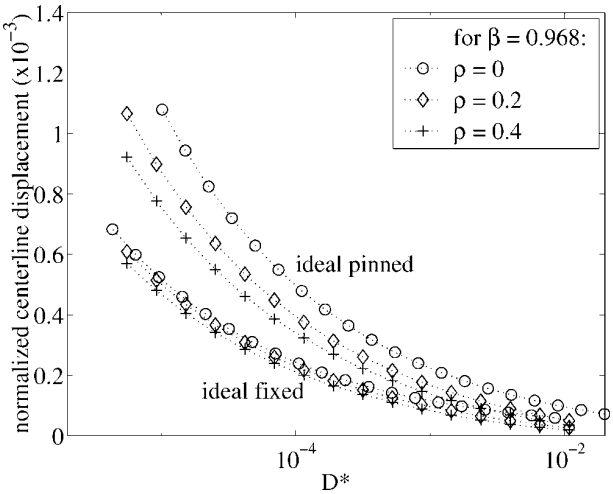

Figure 7. Centerline displacement normalized by passive-plate radius r_p against non-dimensional plate stiffness D^*, at different bonding-to-plate thickness ratios ρ. The curves between the symbols are drawn for clarity.

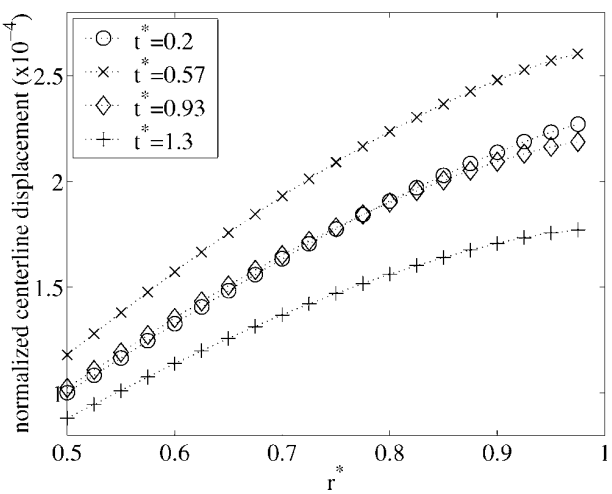

Figure 8. Centerline displacement normalized by passive-plate radius r_p against actuator radius ratio at various actuator thickness ratios, as predicted by the FEA model with the pinned-edge condition for $\alpha = 6$, $\beta = 0.968$ and $\rho = 0$. The curves between the symbols are drawn for clarity.

edge model was also very close. The discontinuities in slope shown by the FEA solutions in figure 10 resulted from the downward strain of the piezoelectric actuator due to the electric field, while the in-plane expansion of the actuator caused upward plate bending. Comparison to centerline displacement was also made for 3 mm diameter pumps, and agreement between FEA and experimental results was within 6.3%.

When the actuators of the two pump sizes studied were optimized using the non-idealized FEA model, the optimum dimensions were close to those of the ideal fixed case in figures 5 and 6. In fact, the values for r^* and t^* were within 11 and 13%, respectively, of the ideal fixed case with $\rho = 0$, given by equations (8) and (9). These results suggest that the design for non-ideal edge supports can be realized with the values for $(r^*)_{opt,fixed}$ and $(t^*)_{opt,fixed}$ from equations (8) and (9). It is reasonable to expect that for larger aspect ratios

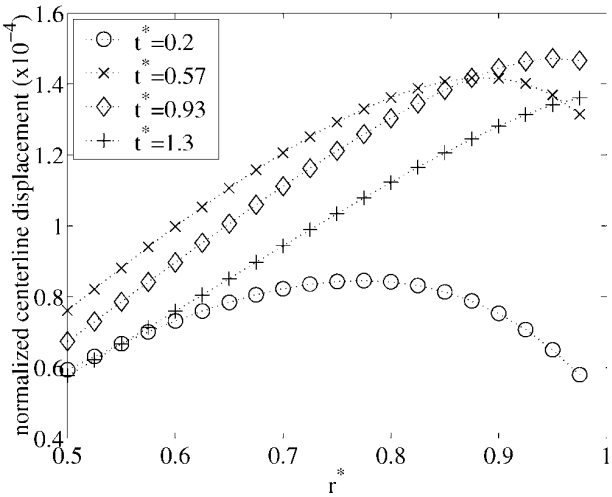

Figure 9. Centerline displacement normalized by passive-plate radius r_p against actuator radius ratio at various actuator thickness ratios, as predicted by the FEA model with the fixed-edge condition for $\alpha = 6$, $\beta = 0.968$ and $\rho = 0$. The curves between the symbols are drawn for clarity.

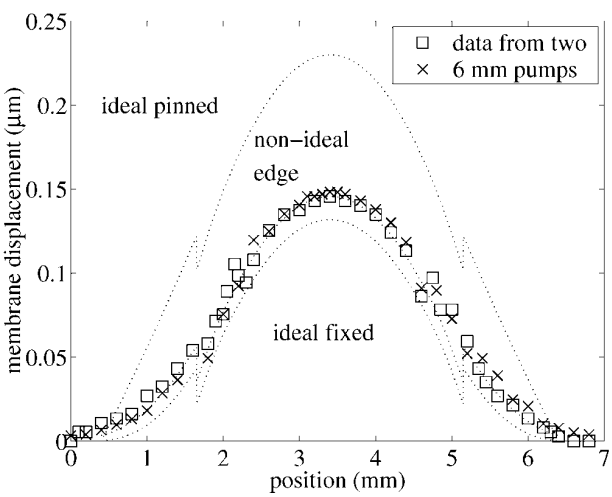

Figure 10. Deflection of bimorph on actuator side from two 6 mm chamber diameter pumps compared to FEA model predictions against the diametrical coordinate, with $\rho = 0.04$. Actuation amplitude is 50 V zero-to-peak.

(large α), the behavior would approach the fixed case even more.

4. Conclusions

When considering the optimum dimensions of a piezoelectric bimorph, one must consider both the geometric and material parameters for the passive plate. To the authors' knowledge no analytical model exists for the single-actuator axisymmetric case. Such a model would be difficult to develop, and at best would accurately predict behavior only in the domain of known edge conditions and negligible bonding layer. The expressions for optimum actuator dimensions given by equations (8) and (9) and the effects of the bonding layer presented in figures 5 and 6 are available for design purposes.

Acknowledgments

This work was partially supported by DARPA Microflumes Program contract N66001-97-C-8632, DARPA Composite CAD Program contract F30602-98-2-0151 and graduate fellowships from the NASA Space Grant and the Boeing Company.

References

ANSYS Theory Reference 1998 9th edn (SAS IP, Inc.)

Auld B A 1973 *Acoustic Fields and Waves in Solids* vol 2 (New York: Wiley) pp 357–72

Bardell R L, Sharma N R, Forster F K, Afromowitz M A and Penny R J 1997 Designing high-performance micro-pumps based on no-moving-parts valves *Microelectromech. Syst.* DSC vol **62**/HTD vol 354 (ASME IMECE) pp 47–53

Batra R C, Liang X Q and Yang J S 1996 Shape control of vibrating simply supported rectangular plates *AIAA J.* **34** 116–22

Chaudhry Z and Rogers C A 1994 Performance and optimization of induced strain actuated structures under external loading *AIAA J.* **32** 1289–94

Chee C Y K, Tong L and Steven G P 1998 A review on the modeling of piezoelectric sensors and actuators incorporated in intelligent structures *J. Intell. Mater. Syst. Struct.* **9** 3–19

Dobrucki A B and Pruchnicki P 1997 Theory of piezoelectric axisymmetric bimorph *Sensors Actuators* A **58** 203–12

Jaffe H and Berlincourt D A 1965 Piezoelectric transducer materials *Proc. IEEE* **53** 1372–86

Kim S J and Jones J D 1991 Optimal design of piezoactuators for active noise and vibration control *AIAA J.* **29** 2047–53

Lee J K and Marcus M A 1981 The deflection-bandwidth product of poly(vinylidene fluoride) benders and related structures *Ferroelectrics* **32** 93–101

Meng Q, Mehregany and Deng K 1993 Modeling of the electromechanical performance of piezoelectric laminated microactuators *J. Micromech. Microeng.* **3** 18–23

Ray M C, Bhattacharya R and Samanta B 1993 Exact solutions for static analysis of intelligent structures *AIAA J.* **31** 1684–91

Roark R J 1989 *Roark's Formulas for Stress and Strain* ed W C Young (New York: McGraw-Hill)

Shah D K, Joshi S P and Chan W S 1993 Static structural response of plates with piezoceramic layers *Smart Mater. Struct.* **2** 172–80

Szücs E 1980 *Similitude and Modeling* (Amsterdam: Elsevier)

Smits J G, Dalke S I and Cooney T K 1991 The constituent equations of piezoelectric bimorphs *Sensors Actuators* A **28** 41–61

Yanagisawa T and Nakagawa Y 1993 Determination of optimum dimensions for unimorph type piezoelectric loudspeaker *Trans. Inst. Electron. Informat. Commun. Eng.* A **J76** 1261–9

Zhang Q M, Wang H and Zhao J 1995 Effect of driving field and temperature on the response behavior of ferroelectric actuator and sensor materials *J. Intell. Mater. Syst. Struct.* **6** 84–93